JOURNAL OF MATERIALS SCIENCE **37** (2002) 5305–5317

Formation and structure of $LiSi_2N_3$-AlN solid solutions

V. ISCHENKO, L. KIENLE, M. JANSEN*
Max-Planck-Institut für Festkörperforschung, 70569 Stuttgart, Germany
E-mail: Hamilton@vsibm1.mpi-stuttgart.mpg.dc

Solid solutions of the composition $Li_xAl_{12-3x}Si_{2x}N_{12}$ ($1 \leq x \leq 3$) have been prepared via a precursor route. According to XRD studies all phases obtained have wurtzite-type substructures with an orthorhombic superstructure related to $LiSi_2N_3$. However, observed powder patterns cannot be adequately described in orthorhombic symmetry, and the significant diffusiveness of the superstructure reflections indicates the presence of disorder. High resolution electron microscopy emphasizes the highly defective nature of the microstructure and the presence of nanoscale domains of apparently varying symmetry. Local ordering of metal ions and slight spatial variations of the composition are assumed to be possible reasons for the long-range inconsistencies of the structures. The Li^+ ion conductivity, as measured on selected solid solutions, is lower, than that of $LiSi_2N_3$.
© *2002 Kluwer Academic Publishers*

1. Introduction

The outstanding chemical, thermal and mechanical properties of silicon nitride, due to an extreme stability of covalent bonds in its highly cross-linked structure, have recently evoked interest toward nitridosilicates M-Si-N [1–4]. However, unlike the situation with oxosilicates M-Si-O and oxonitridosilicates M-Si-N-O, binary or multinary nitridosilicates have been synthesized in limited number, only [1]. The reason is that even at high temperatures Si_3N_4 is so inert that it only reacts with the most basic and reactive metal nitrides (e.g., Li_3N, Mg_2N_3). This problem has recently been overcome by a new synthetic approach based on the interaction of various metals with silicon diimide $Si(NH)_2$, thus enabling the preparation of ternary M-Si-N and quaternary M-Ln-Si-N nitrides (with M = alkali earth, and Ln = rare earth metals) [2].

In spite of the growing importance of covalent nitride ceramics for application (e.g., Si-B-C-N [3, 4]), metal nitridosilicates are only scarcely used in technology. Among them lithium silicon nitrides, manifesting high values of ionic conductivity, could be of the most practical interest. The ionic conductivity of these compounds increases with the amount of lithium ions in the tetrahedral interstices of h.c.p. formed by nitrogen. $LiSi_2N_3$, in which half of the tetrahedral cavities are occupied, could not accommodate more metal atoms without changing to a c.c.p. structure, in which all tetrahedral and even a part of octahedral interstices could be occupied. The limiting composition that has been reached is Li_8SiN_4 [5]. The ionic conductivity increases in this case from 1.9×10^{-5} S/m (400 K, $LiSi_2N_3$) up to 5×10^{-2} S/m (400 K, Li_8SiN_4), the latter being the highest for lithium ion conductors with antifluorite structure [5].

If the limit conductivity connected with a maximal possible amount of lithium in the structure is reached, another alternative way to create materials with high values of ionic conductivity becomes more important: a modification of the microstructure. The possibility for conductivity enhancement (up to several orders of magnitude) has been demonstrated in composite solid electrolytes, prepared by dispersing submicrometer-size particles of insulating and inert materials into a moderate-ionic conducting solid [6, 7]. In this case, the decomposition of solid solutions seems to be the most promising way to introduce second-phase dispersions into a host matrix, allowing a fine tuning of the size and providing higher uniformity of their distribution. Recent investigations of the bulk conductivity of $LiFe_5O_8$-$LiAl_5O_8$ solid solutions, undergoing spinodal decomposition, showed that there is a maximum in bulk conductivity corresponding to the initial segregation of the insulating phase $LiAl_5O_8$ [8]. Similarly, an enhancement of the ionic conductivity has been observed with initial formation of ordered, poorly conducting domains in Y_2O_3-ZrO_2, Y_2O_3-ZrO_2-TiO_2 and Y_2O_3-ZrO_2-Nb_2O_5 solid solutions [9]. Thus, the formation of nanostructured materials, based on lithium silicon nitrides, prepared by decomposition of quaternary solid solutions Li-M-Si-N should undoubtedly attract the attention of researchers.

Hitherto, no lithium-containing quaternary nitridosilicate (Li-M-Si-N) has been synthesized (the oxygen containing Li-sialons are not considered here), although the possibility to form some other quaternary

---

[*] Author to whom all correspondence should be addressed.

0022–2461 © *2002 Kluwer Academic Publishers*

nitridosilicates, like $MgAlSiN_3$, $CaAlSiN_3$, $MnAlSiN_3$ [10] and AlN-$BeSiN_2$ solid solutions [11], all having wurtzite-type structure, has been mentioned in the literature. Further examples are $Ca_{1.83}Si_{8.34}Al_{3.66}N_{16}$ (α'-Si_3N_4-type structure) [12] and different M-Ln-Si-N nitrides (M = Sr, Ba/Eu; Ln = Yb, Nd) [2, 13, 14]. Obviously, the preparation of Li-containing quaternary nitridosilicates requires, on one hand, high temperatures to react all components and, on the other hand, low temperatures to prevent weight loss of lithium before its assimilation by the crystal structure of the product.

In this work, we have prepared solid solutions $LiSi_2N_3$-AlN and investigated their microstructure. Both AlN and $LiSi_2N_3$ have wurtzite-type crystal structure, thus unlimited solubility between these compounds is expected. To provide the highest degree of component homogeneity and to decrease the synthesis temperature, polymeric amide precursors have been synthesized, first.

2. Experimental

The polymeric amide precursors have been obtained by the reaction of different molar ratios of lithium aluminum hydride $LiAlH_4$ (Merck >97%; additionally recrystallized from diethyl ether) with melted tetrakis(methylamino)-silane $Si(NHCH_3)_4$ (preparation see [15, 16]) at 50°C for 1 hr under stirring in argon atmosphere. An intense evolution of hydrogen was observed in the course of the reaction. To provide better cross-linking of the oligomers obtained, the reaction mixture was heated in a flow of ammonia at 150°C for 3 hrs. The resulting polymeric product was a colorless glassy solid of the bulk composition $Li_nAl_nSi_m(NCH_3)_x(NHCH_3)_y$, with $n{:}m$ ratio corresponding to the molar ratio of the reactants, and with varying x and y.

Further ammonolysis of the polymeric precursors was carried out in molybdenum boats at 900°C for 10 hrs in ammonia flow, to allow elimination of $-CH_3$ groups (determined max. carbon content after treatment ~0.05 at.%). Finally, the thermal decomposition, leading to cleavage and elimination of imido- and amidogroups, was carried out in covered tantalum containers at 1300°C for 3 hrs in argon flow, resulting in the formation of $Li_xAl_{12-3x}Si_{2x}N_{12}$. According to elemental analysis data, there was no contamination of the samples by molybdenum or tantalum.

The samples were examined by powder X-ray diffraction (XRD) with a STOE STADI P diffractometer (transmission mode, germanium monochromator, using Cu K_α radiation). Elemental maps were obtained with a PHILIPS XL30TMP scanning electron microscope.

Two samples were characterized by high resolution electron microscopy (HREM) and selected area diffraction (SAD). The preparation of the samples for HREM was performed in a glove box under dry argon. The samples were crushed in an agate mortar to obtain thin transmittable crystallites which were randomly oriented on a perforate carbon/copper net. These nets were fixed in a side-entry, double tilt holder, with a maximum tilt-angle of ±25°. The electron microscopy studies were performed with a Philips CM30/ST microscope (spherical aberration constant $C_S = 1.15$ mm) equipped with

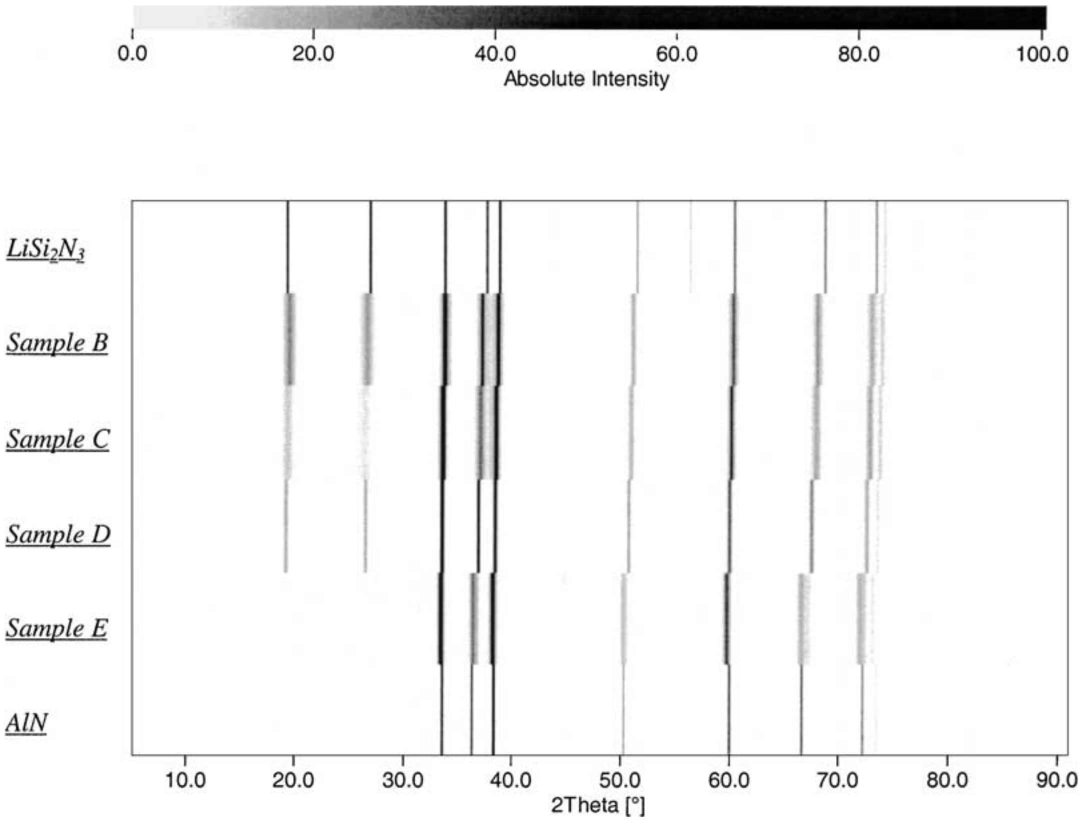

Figure 1 XRD patterns of the samples B, C, D and E after annealing at 1300°C for 3 hrs. For the comparison, calculated theoretical patterns for $LiSi_2N_3$ (ICSD-34118) and AlN (ICSD-82790) are included.

a LaB_6-cathode. Operating at 300 kV the point resolution is 0.19 nm. SAD patterns were obtained using a diaphragm which limited diffraction from a region of the selected crystallite of 125 nm in diameter. Simulations of kinematical electron diffraction patterns and of HREM images (multislice formalism, spread of focus $\Delta = 7$ nm, illumination semiangle $\alpha = 1.2$ m rad) were calculated with the EMS program package [17].

Ionic conductivity measurements were carried out on the pressed samples placed between silver cylinders over a temperature range from 30 to 700°C in argon. The AC impedance of the samples was measured over the range $5\text{ Hz} < f < 1.3 \cdot 10^7$ Hz using a HP 4192A impedance analyzer; the electronic contribution to the conductivity was determined by DC measurements using a HAMEG 8112 multimeter.

3. Results and discussion

3.1. Chemical and phase composition

Samples of five different stoichiometries have been prepared, the chemical compositions of which were studied before and after high temperature annealing (Table I). A significant weight loss of lithium due to evaporation has been noted in the *samples D* and *E* after treatment at 1300°C for 3 hrs. The oxygen content was found not to exceed 1.2 at.% in all samples.

TABLE I Initial and final stoichiometry the prepared samples

Sample	Initial ratio Li:Al:Si	Final ratio Li:Al:Si	Final bulk composition	Cation:Anion
A	0.2 : 0.2 : 1	0.2 : 0.2 : 1	$Li_{1.5}Al_{1.5}Si_{7.5}N_{12}$	0.88 : 1.00
B	0.4 : 0.4 : 1	0.4 : 0.4 : 1	$Li_{2.5}Al_{2.5}Si_{6.3}N_{12}$	0.94 : 1.00
C	0.5 : 0.5 : 1	0.5 : 0.5 : 1	$Li_{3.0}Al_{3.0}Si_{6.0}N_{12}$	1.00 : 1.00
D	0.7 : 0.7 : 1	0.5 : 0.7 : 1	$Li_{2.8}Al_{3.7}Si_{5.5}N_{12}$	1.00 : 1.00
E	3.0 : 3.0 : 1	0.5 : 3.0 : 1	$Li_{1.4}Al_{8.0}Si_{2.7}N_{12}$	1.01 : 1.00

The XRD analysis of samples annealed at 1300°C for 3 hrs has shown that, with the exception of *sample A*, they are single-phase, and their diffraction patterns suggest orthorhombically distorted wurtzite crystal structures, similar to that of $LiSi_2N_3$ (Fig. 1). A consistent shift of the lattice parameters, with increasing aluminum content, confirms the formation of solid solutions.

It should be noted, that a synthetic approach based on the interaction of $LiAlH_4$ with $Si(NHCH_3)_4$ puts some limitations on the stoichiometry of the polymeric amide precursors. The only possible cation ratios are those lying on the dashed line connecting Si_3N_4 and $[LiN_{1/3} \cdot AlN]$ (Fig. 2). The loss of lithium in *samples D* and *E* during high temperature annealing thus leads to a shift of their cation stoichiometry to the *points D′* and *E′*, approaching the proposed line of solid solutions $LiSi_2N_3$-AlN. The elemental analysis confirms, that the ratio of Al:Si remains unchanged and that the cation to anion ratio in the *samples D* and *E* approaches 1:1 (Table I).

The compositional decay, leading to the formation of a solid solution $Li_xAl_{12-3x}Si_{2x}N_{12}$ and Si_3N_4, could be expected for the *sample B*, lying below the line of solid solutions $LiSi_2N_3$-AlN. However, the formation of the single phase is observed for this sample as well, suggesting the stability of cation deficient $Li_{2.5}Al_{2.5}Si_{6.3}N_{12}$ solid solution. Yet it maintains a wurtzite-derived crystal structure, the general formula corresponding to $M_{0.94}\square_{0.06}X$ (where $\square \equiv$ cation vacancy).

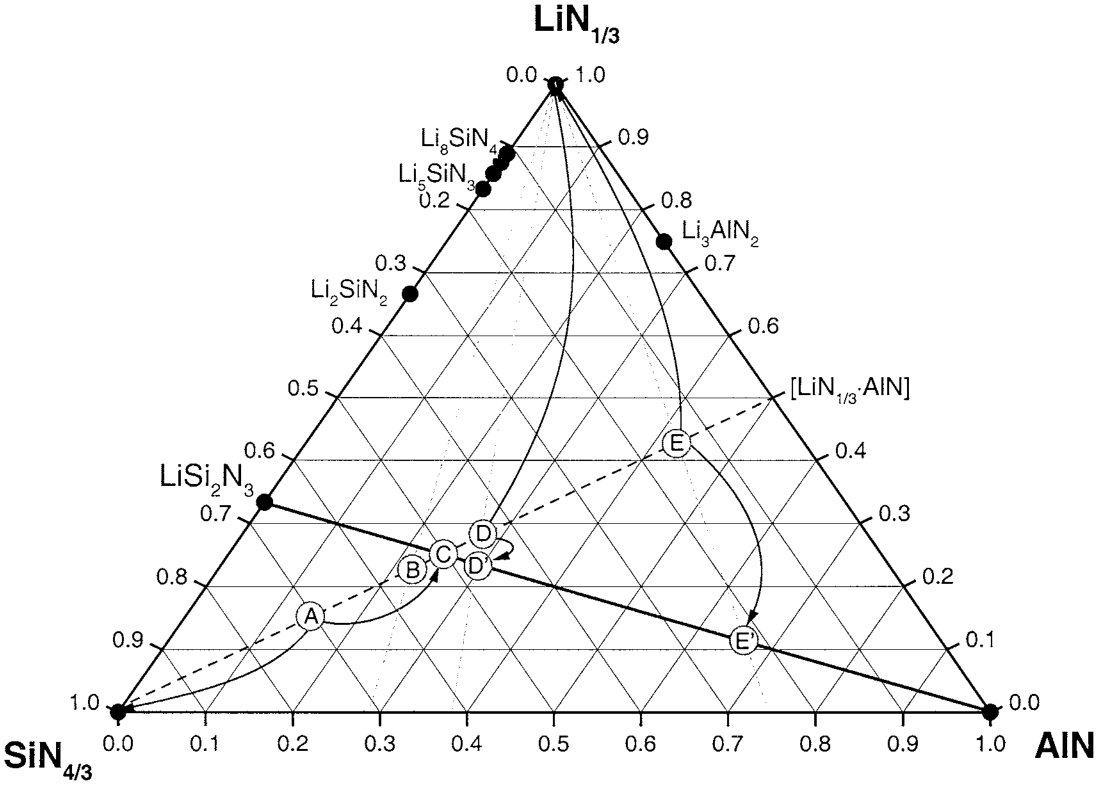

Figure 2 The positioning of cation stoichiometries for the studied samples, relative to Li_3N-AlN-Si_3N_4 ternary phase diagram, before annealing at 1300°C (points A, B, C, D and E) and the occurring compositional decay during the annealing (indicated by arrows) are shown. The line connecting $LiSi_2N_3$ and AlN corresponds to the proposed region of solid solution formation.

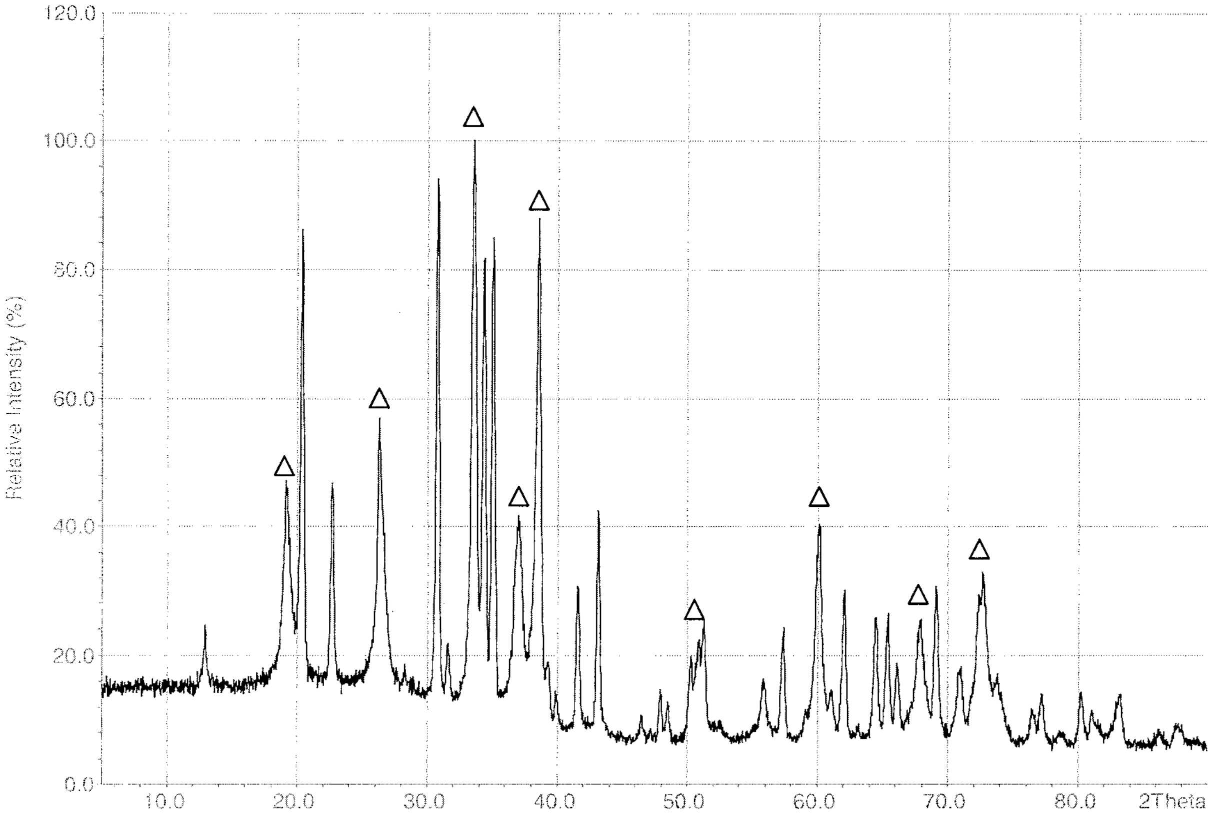

Figure 3 XRD pattern of the sample A after annealing at 1300°C for 3 hrs. (Δ- peaks related to $Li_xAl_{12-3x}Si_{2x}N_{12}$ solid solution; all unmarked peaks correspond to α-Si_3N_4.)

A stronger deviation of the cation ratio from the line of $LiSi_2N_3$-AlN solid solution (*sample A*), leads, finally, to the formation of two phases, by which the above mentioned compositional decay to $Li_xAl_{12-3x}Si_{2x}N_{12}$ ($x = 3$) solid solution (corresponding to *point C*) and to α-Si_3N_4 occurs (Fig. 3).

3.2. Microstructure features

For the compounds attaining a wurtzite-derived crystal structure and containing several types of metal atoms, there are the possibilities of either statistical or ordered arrangement of them. Wholly statistical arrangement leads to undistorted hexagonal symmetry ($P6_3mc$), while an ordering of metal atoms with different radii would lead to some type of distortion–first of all, an orthorhombic distortion to *mm*2 symmetry is expected. The presence of superstructure peaks in the region of $2\theta < 30°$ in the XRD patterns of the *samples B*, *C*, *D* and *E* is indicating, that pure hexagonal symmetry does not appear for the $LiSi_2N_3$-AlN solid solutions. Thus, some sort of metal atoms ordering is assumed in these samples.

If the ordering occurs, the replacement of aluminum in AlN by two other metal atoms, one of which is silicon, could lead to the formation of several superstructures:

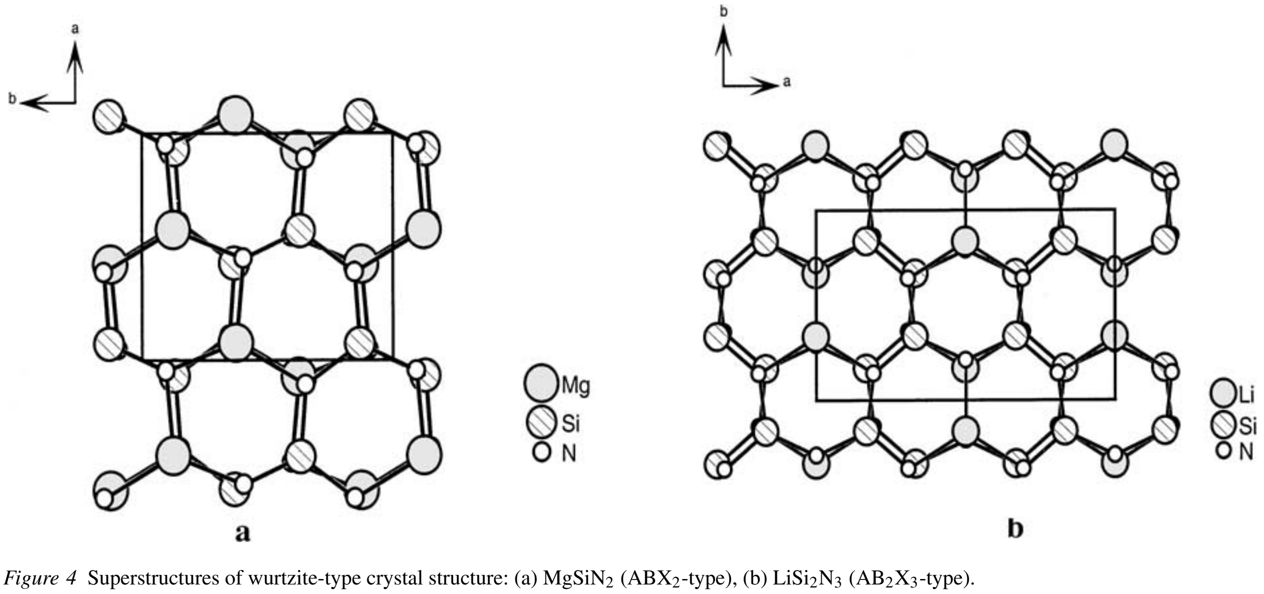

Figure 4 Superstructures of wurtzite-type crystal structure: (a) $MgSiN_2$ (ABX_2-type), (b) $LiSi_2N_3$ (AB_2X_3-type).

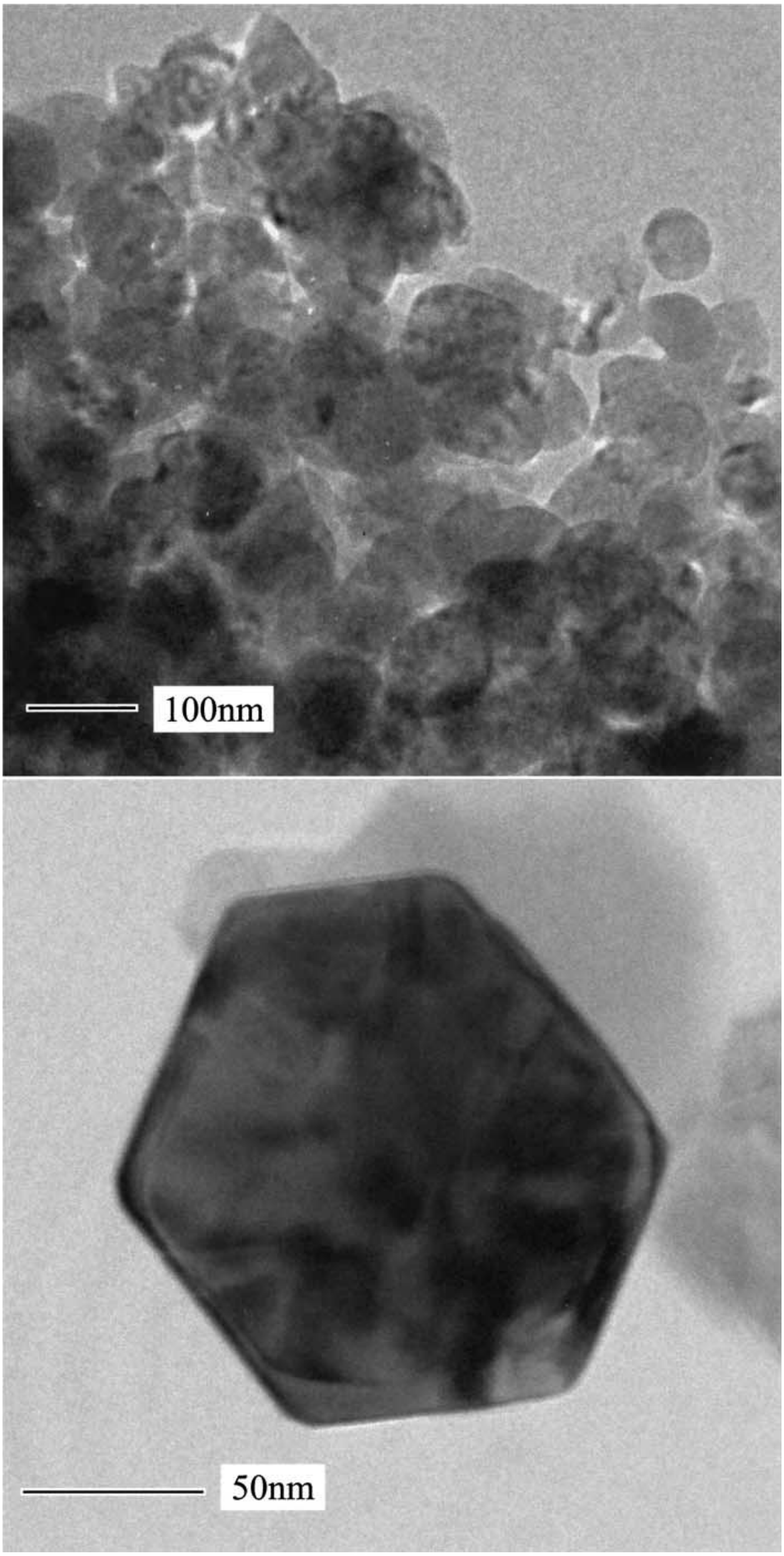

Figure 5 Typical TEM micrograph of a conglomerate of nanosized particles (top) and pseudohexagonal nanocrystal (bottom).

$$\mathrm{MX}\ \begin{array}{l} \nearrow\ \mathrm{ABX_2} \Rightarrow \mathrm{M^{II}SiN_2} \\ \rightarrow\ \mathrm{AB_2X_3} \Rightarrow \mathrm{M^{I}Si_2N_3}\ ,\ \mathrm{M^{II}AlSiN_3} \\ \overset{?}{\searrow}\ \mathrm{AB_3X_4} \Rightarrow \mathrm{M^{I}AlSi_2N_4}\ ,\ \mathrm{M^{II}Al_2SiN_4} \end{array}$$

Compounds of the composition $M^{II}SiN_2$ (with M = Be, Mg, Mn) are known to form an orthorhombic superlattice (space group $Pna2_1$) [10] related to the hexagonal AlN cell by:

$$a_{\mathrm{ortho}} \approx \sqrt{3}a_{\mathrm{hex}}, \quad b_{\mathrm{ortho}} \approx 2a_{\mathrm{hex}}, \quad c_{\mathrm{ortho}} \approx c_{\mathrm{hex}}$$

(see Fig. 4a). Compounds $M^{I}Si_2N_3$ and $M^{II}AlSiN_3$ (with M^{I} = Li; M^{II} = Be, Mg, Mn, Ca) have a

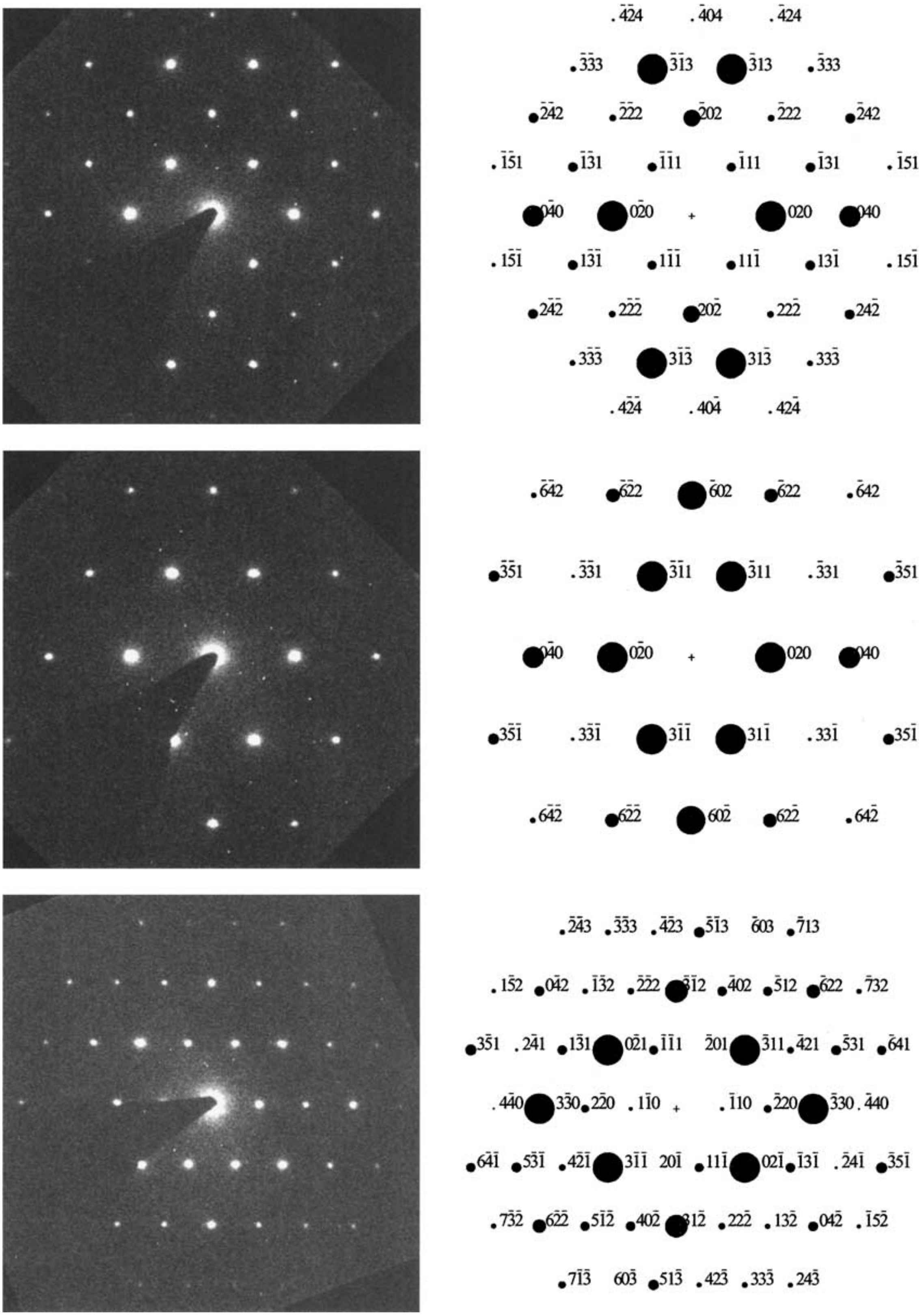

Figure 6 Examples of SAD patterns obtained in the framework of the tilting experiments. Zone axis orientation [101] (top), [103] (middle) and [112] (bottom).

different orthorhombic superlattice of AlN (space group $Cmc2_1$) [10] with M atoms in position $4a$, Si and Al sharing position $8a$, and with:

$$a_{\text{ortho}} \approx 3a_{\text{hex}}, \quad b_{\text{ortho}} \approx \sqrt{3}a_{\text{hex}}, c_{\text{ortho}} \approx c_{\text{hex}}$$

(see Fig. 4b).

The third type of compositions, for which a wurtzite-superstructure could be expected, includes two possible compounds $\text{M}^{\text{I}}\text{AlSi}_2\text{N}_4$ and $\text{M}^{\text{II}}\text{Al}_2\text{SiN}_4$ which are not known from the literature. The existence of complete solubility between BeSiN_2 and AlN implies in principle the possibility to form $\text{BeAl}_2\text{SiN}_4$. However, no ordering has been observed for $\text{Be}_{1-x}\text{Si}_{1-x}\text{Al}_{2x}\text{N}_2$ solid solutions in the range $0 < x < 1$, suggesting completely disordered hexagonal wurtzite-type crystal structure [11]. The low diffusion rate is considered to be the reason for the atoms not to order. The other compound mentioned, $\text{M}^{\text{I}}\text{AlSi}_2\text{N}_4$ (with $\text{M}^{\text{I}} = \text{Li}$), is a member of a row of solid solutions $\text{Li}_x\text{Al}_{12-3x}\text{Si}_{2x}\text{N}_{12}$, studied in this work (see *sample C*).

The peak positions in powder XRD patterns for the *samples B*, *C*, *D* and *E* suggest that a wurtzite-superstructure AB_2X_3 (space group $Cmc2_1$)

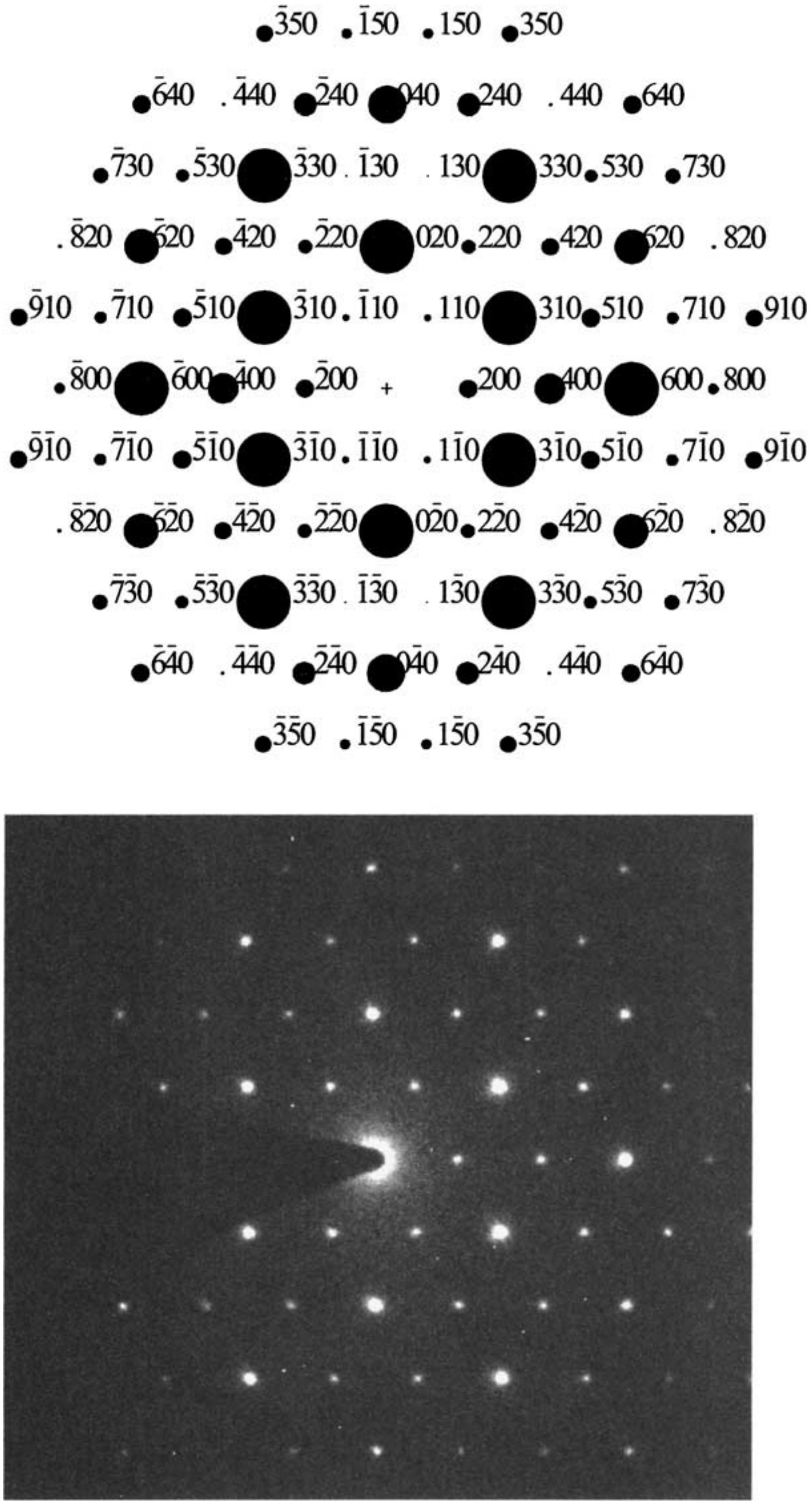

Figure 7 Simulated (top) and experimental SAD pattern (bottom) with zone axis orientation [001].

is formed by all of them. Nevertheless, the comparison with calculated theoretical patterns showed that observed intensity relations correspond neither to a fully ordered structure—with one atom type in position 4*a*, another in position 8*a* and the third one being statistically disordered on these positions,—nor to a fully disordered structure with all metal atoms equally distributed over positions 4*a* and 8*a*. Thus, the intermediate situation with partial or local ordering of metal atoms in 4*a* and 8*a* has to be assumed.

All attempts to index the patterns for the single phase samples in the orthorhombic crystal system failed, suggesting that the crystal structure might be distorted, and, therefore, the symmetry be lower than orthorhombic. Another possible explanation is that these solid solutions possess an irregular microstructure, distorted by extended defects or microdomains with symmetry, and probably composition, variations. Very high FWHM values (about 0.4–0.5°), especially for superstructure reflections (200), (110) and (111), observed even after additional annealing of the samples at 1300°C for up to 10 hrs, support the latter assumption as well. Similarly, the structure refinements reported for $MgAlSiN_3$ and for $MnAlSiN_3$ did not give entirely satisfactory *R*-values for reasons not currently apparent [10].

It has already been realized in the past that high temperature sintering does not work very well in the case of oxygen-free covalent nitrides containing Si-N bonds. To achieve a significant diffusion rate in these ceramics, some amount of oxygen should be present to form an oxonitride liquid on the surface of the crystallites at the temperature of sintering. Therefore, in attempting to improve the crystallinity, a part of the *sample C* has been partially oxidized, by exposing it to air for several minutes before annealing at 1300°C (denoted as *"sample C-ox"*). The oxygen content in the *sample C-ox* was found to be 6.1 at.%. This treatment led to a decrease of FWHM values after annealing at 1300°C to 0.2–0.3° 2θ, with retaining the crystal structure similar to non-oxidized *sample C*. The profile matching for this sample in $Cmc2_1$ converged at $R_p = 8.79\%$ and $R_{wp} = 16.79\%$, with cell parameters $a = 9.260$ Å, $b = 5.333$ Å, $c = 4.869$ Å.

To elucidate the defect structure and prove the possibility of local ordering of metal atoms in $LiSi_2N_3$-AlN solid solutions, *samples C* (0.8 at.% O) and *C-ox*

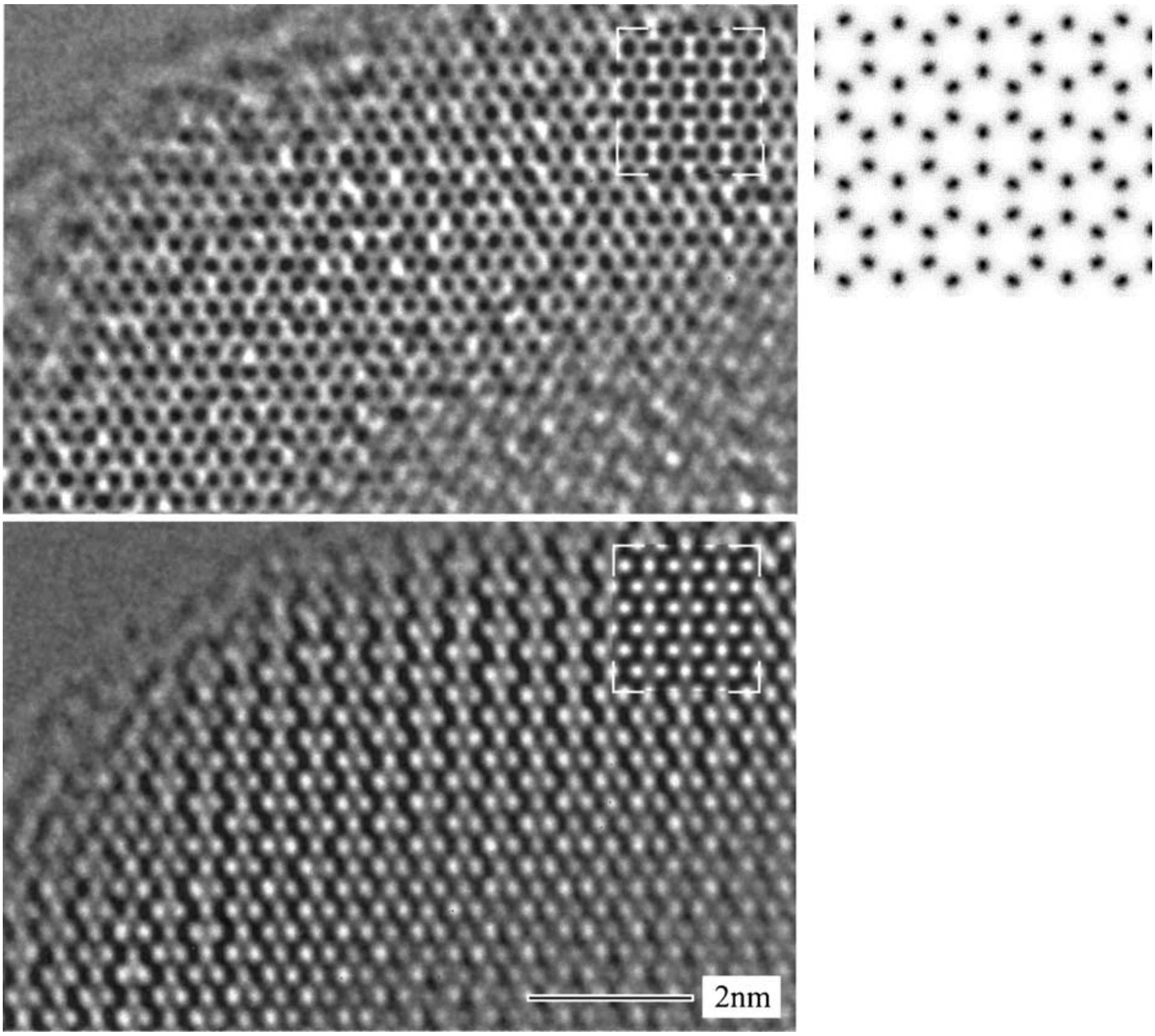

Figure 8 Left: HREM micrograps, zone axis [001] with variable defocus ($\Delta f = -20$ nm (top), and $\Delta f = -35$ nm (bottom)), simulations inserted (thickness: 2.4 nm). Right: projected crystal potential.

(6.1 at.% O), having the simple integer-numbered ratio of cations (Li : Al : Si = 1 : 1 : 2), have been studied by high resolution electron microscopy.

All electron diffraction patterns have been obtained while performing tilting experiments and could completely be indexed on the basis of a disordered structure model (see Table II), which is related to the orthorhombic structure of $LiSi_2N_3$. This structure model serves as a basis for computer simulations and identification of the zone axis. The cations M occupy tetrahedral cavities in statistical disorder. The ratio of the occupancy factors G(Li) : G(Al) : G(Si) is 1:1:2 for all positions.

TABLE II Orthorhombic structure model of $LiAlSi_2N_4$ ($Cmc2_1$, lattice parameters [nm]: $a = 0.9260$, $b = 0.5333$, $c = 0.4869$, $V = 0.2405$ nm^3)

Atom	x	y	z
M1	0	0.333	0
M2	0.168	0.834	0.984
N1	0.192	0.860	0.348
N2	0	0.290	0.424

The shape and size of the particles is very similar for *sample C* and *C-ox*. A conglomeration of irregular oval particles in the range of 40–140 nm is shown in the typical TEM micrograph in the upper part of Fig. 5. All particles are crystalline, no amorphous byproducts or larger amorphous regions in the nanoscaled crystals were observed. Some of the crystallites exhibit a well defined morphology with sharp edges, especially when aligned (Fig. 5, bottom) in the zone axis orientation [001]. These aligned crystals possess approximately the shape of a hexagonal plate. As indicated by electron diffraction the vertical axis of those plates is [001].

In order to check the symmetry of selected crystals electron diffraction and HREM analyses were performed. The observations emphasize the main difference between both samples. Only in the case of *sample C-ox* the crystallites do not exhibit any defects. Electron diffraction patterns of thin regions of the crystallites agree reasonably well with the calculated ones, assuming the orthorhombic structure (examples presented in Fig. 6). However, the exceptions are found in the observed patterns with the zone axis orientation [001],

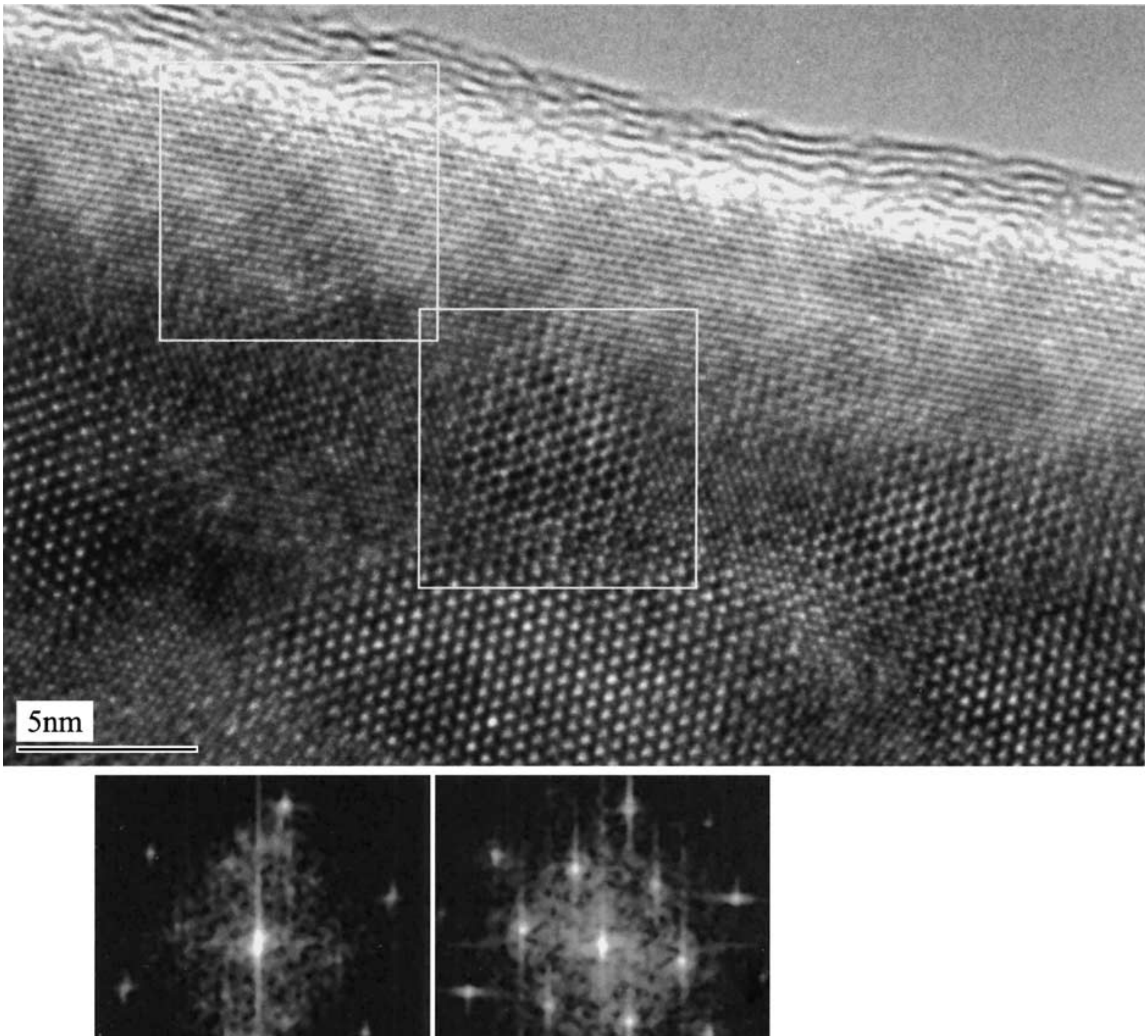

Figure 9 HREM image of a domain crystal (sample C), zone axis [001] with Fourier transforms of selected regions (see marks in the HREM image).

showing in juxtaposition to the calculated pattern a perfect hexagonal distribution of the intensities (see Fig. 7). Multiple twinning, which could produce a hexagonal symmetry as an artifact by superposition of three orthorhombic domains has not been found. An unambiguous distinction between hexagonal and orthorhombic symmetry is possible by HREM. The pseudo-hexagonal symmetry of the orthorhombic structure (orientation [001]) is also emphasized by the projected potential (Fig. 8). On the whole, the deviations of simulated and experimental images from a regular hexagonal structure are very small and depend significantly on the crystal thickness and the defocus value. In the HREM micrographs of Fig. 8 the orthorhombic symmetry of the structure is noticeably visible only for $\Delta f = -35$ nm. Thus the existing orthorhombic structure should be very close to hexagonal symmetry.

The HREM images observed for the crystals of *sample C* could not be interpreted on the basis of a simple three-dimensional structure model. In this case we found a complex structure of microdomains with sizes of several nanometers. This domain structure of the crystallites leads to considerable shifts of the contrasts in HREM images. The single microdomains are also characterized by significant changes in the Fourier transforms, see Fig. 9. These Fourier transforms give a first hint, that microdomains with another symmetry than an orthorhombic one are present within the same crystallite.

Also, between neighboring microdomains with equal Fourier transforms crystal defects could be detected. Especially for those zone axis orientations with [001] perpendicular to the beam direction crystal defects could be observed. These defects are defined by a shift

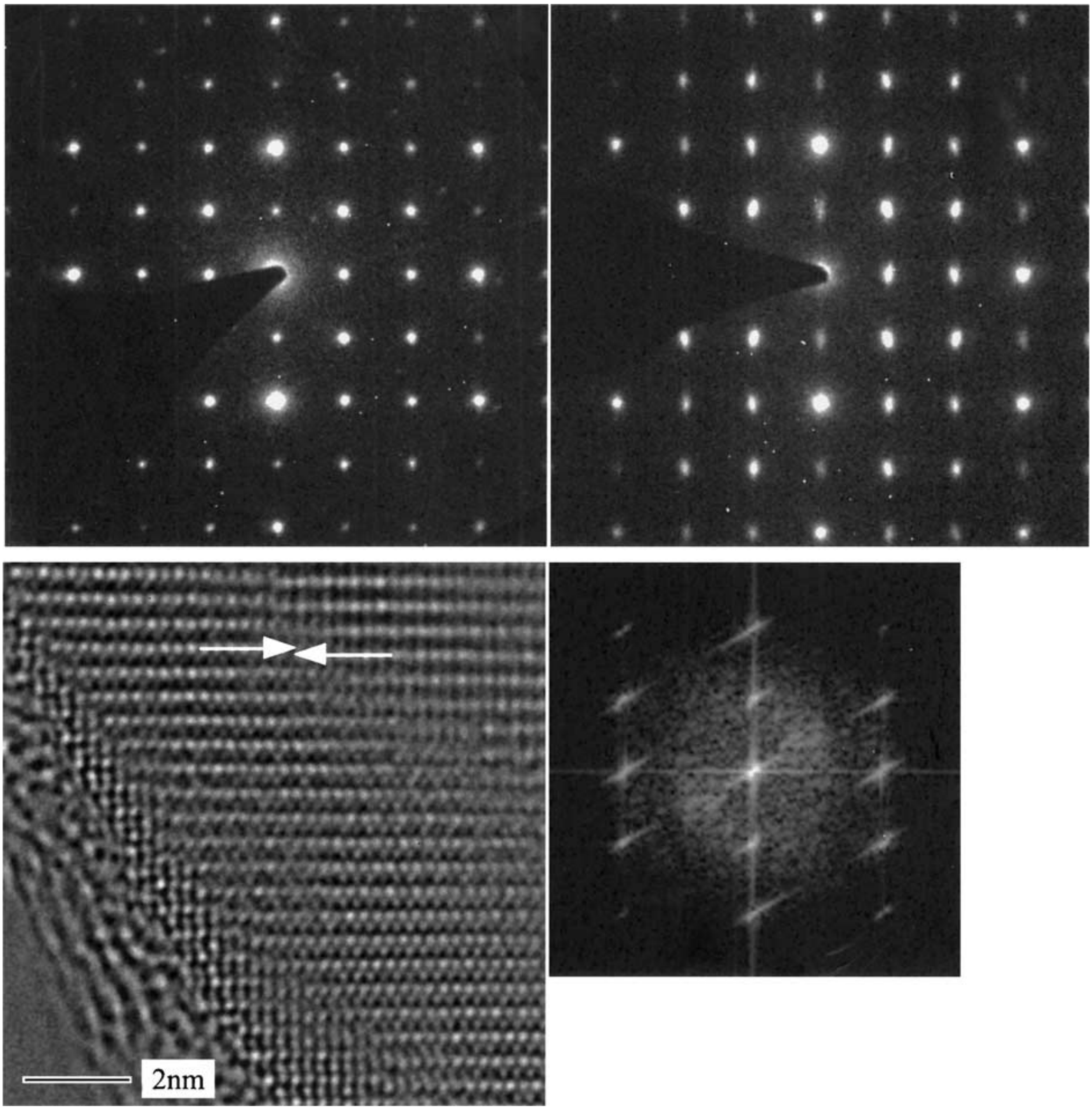

Figure 10 Top: SAD patterns, zone axis [110], of an undistorted crystals (left, sample *C-ox*, no diffuse scattering) and a distorted crystal (right, sample C, diffuse elongation of the Bragg reflections in [001]*). Bottom: HREM image of a crystal defect (left), orientation [130]. As indicated by the arrows, the microdomains are shifted by approximately $1/2|\vec{c}|$. Right: Fourier transform of the image.

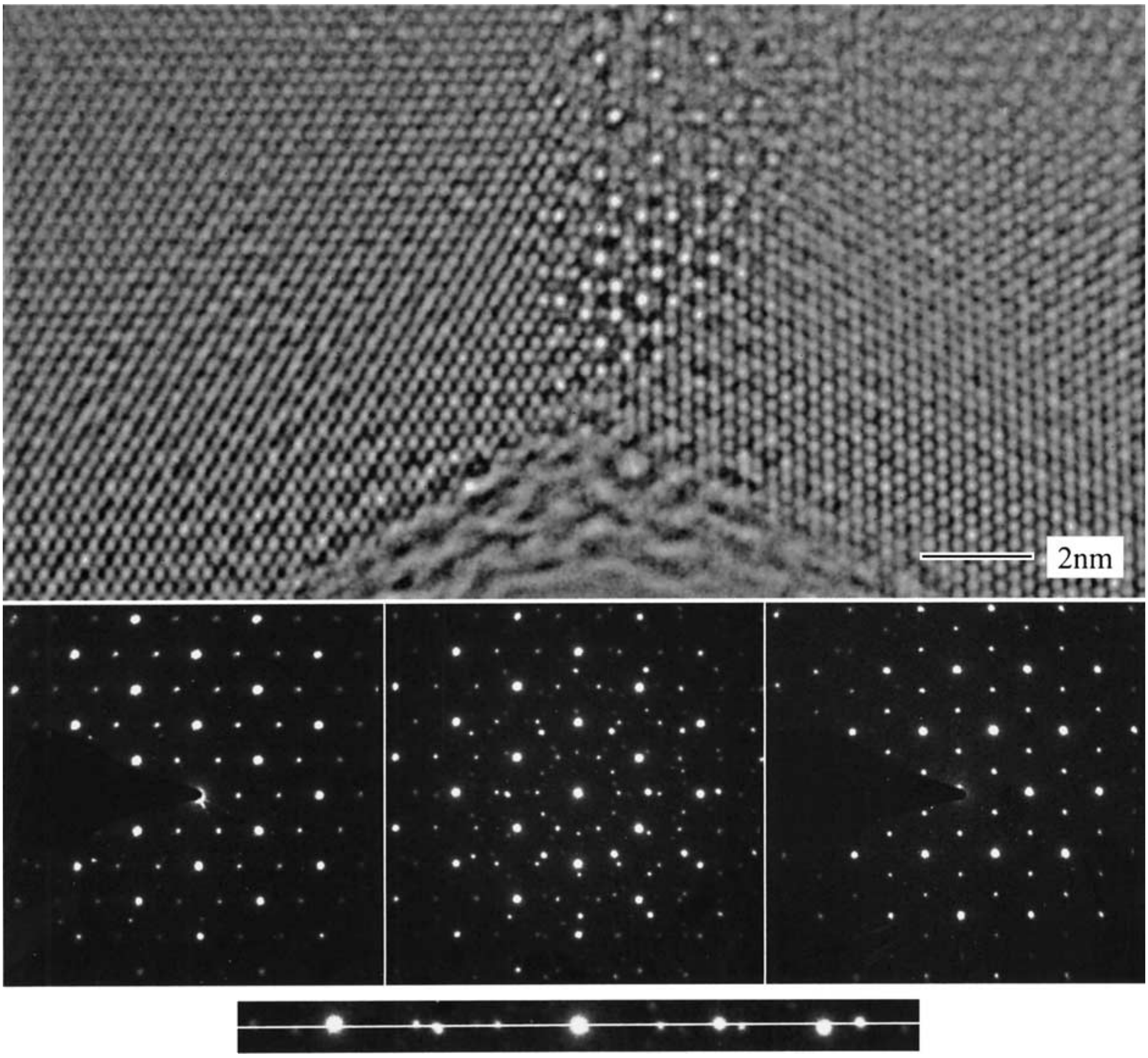

Figure 11 Top: HREM image of the twin domains, zone axis [001]. Middle: SAD patterns of the different regions of the twinned crystal (left: domain 1, middle: overlap of domain 1 and 2, right: domain 2). Bottom: enlarged section of the SAD pattern taken in the region of the overlapping domains. The reflections of the two domains cannot be connected by the displayed line, which represents the directions $[100]^*_1$ or $[010]^*_2$.

of the domains in [001] and are manifested by a diffuse elongation of the Bragg reflections in electron diffraction patterns and Fourier transforms in the direction [001]* (displayed in Fig. 10 for [110] and [130]). By HREM this shift is determined to approximately $1/2|\vec{c}|$, see the HREM image in Fig. 10 bottom left for the orientation [130]. Finally we come to the conclusion, that the great variety of contrasts depends strongly on the overlap of microdomains with partly different symmetry. Frequently even microdomains with equal symmetry are not ideally compatible and therefore cannot be superimposed without the production of crystal defects.

Another interesting, but only rarely observed, feature of the real structure which is limited to *sample C* are twin boundaries. The upper part of Fig. 11 shows the separated domains in the left and right part of the HREM image. The corresponding diffraction patterns are displayed in the lower part. The intersection of the tilted domains results in superposition, which is visible in the center parts of the HREM image and the corresponding SAD pattern. At first glance the twin domains are connected by a rotation of 90° around [001], and therefore they should be described as pseudo-merohedral twins. On closer inspection of diffraction patterns in the orientation [001], there is only an approximate coincidence of the reciprocal directions $[100]^*_{\text{domain 1}}$ with $[010]^*_{\text{domain 2}}$ and $[100]^*_{\text{domain 2}}$ with $[010]^*_{\text{domain 1}}$, respectively, see Fig. 11 bottom. Hence we concluded that these twins must be described as rotation twins, with the twin axis [530]*. The deviations from a perfect pseudo-merohedry could be quantified: the angle of 46.2° between [100]* and [530]* (instead of 45° for perfect twining by pseudo-merohedry) is responsible for these small distortions.

3.3. Electrochemical properties

The total conductivities of the samples were measured by the complex impedance method. The electronic contribution was found to grow with an increase of the aluminum content in the sample, being, however, less than 10% for *sample E* and less than 1% for *samples B*, *C* and *D*. Thus, most of the conductivity is caused by the migration of lithium ions.

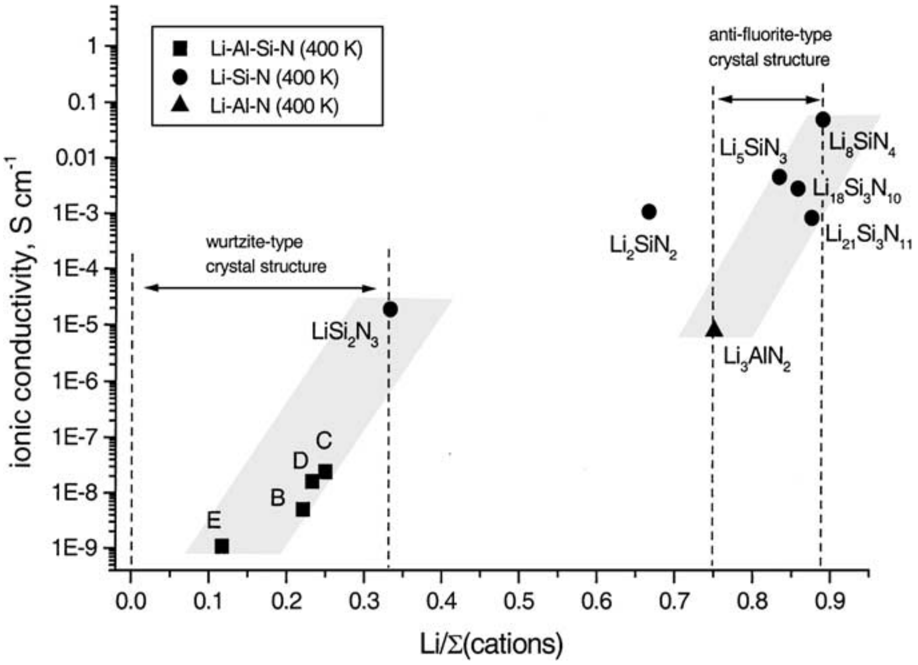

Figure 12 Comparison of the ionic conductivity values measured at 400 K for $LiSi_2N_3$-AlN solid solutions (samples B, C, D and E), Li_3AlN_2 [18] and lithium nitridosilicates Li-Si-N [5].

The ionic conductivity of solid solutions $LiSi_2N_3$-AlN has been measured to be significantly lower than that of $LiSi_2N_3$. The lower amount of lithium is assumed to be the main reason for deterioration of the ionic conductivity. A direct correlation between lithium content and ionic conductivity in Li-Al-Si-N system can be readily seen from Fig. 12. An increase of activation energy is observed for the samples under discussion, being in the range of 68–80 kJ/mol, compared with 64 kJ/mol for $LiSi_2N_3$ [5].

4. Conclusion

The formation of solid solutions between $LiSi_2N_3$ and AlN has been observed during thermal decomposition of polymeric amides. The obtained samples with bulk composition $Li_xAl_{12-3x}Si_{2x}N_{12}$ $(1 \leq x \leq 3)$ possess wurtzite-derived crystal structures with an orthorhombic superstructure related to $LiSi_2N_3$. The comparison of intensity relations in various theoretical models and observed patterns suggests that in space group $Cmc2_1$ every metal atom type could occupy both positions, $4a$ and $8a$, although their distribution is not completely random, and preferred ordering of Li atoms at $4a$ is assumed. Thus, the structure can be regarded as partially or locally ordered. Structure refinement for the samples obtained showed that there is an obvious bulk inconsistency of the crystal structure connected with quite diffuse superstructure reflections; as a consequence, reasonable R-values cannot be achieved.

The examination of $Li_xAl_{12-3x}Si_{2x}N_{12}$ samples with metal atom ratio 1 Li : 1 Al : 2 Si by high resolution electron microscopy revealed the existence of nano-sized crystallites with a high defect content and complex microdomain structure. By partly substituting nitrogen for oxygen, the diffusion rate at the temperature of annealing can be increased, leading to accelerated elimination of extended defects. Most of the observed defects in the low-oxygen content sample are obviously connected with a shift of the domains along [001]. Taking into account possible slight deviations of the M:X ratio from 1:1, the locally formed wurtzite-based Ramsdell polytypoid structures M_nX_{n+1} or antipolytypoid structures $M_{n+1}X_n$ with high n values can be assumed to be responsible for the defects formation along [001]. Such deviations could occur due to deficiency or, on the contrary, due to excess of lithium in the structure, or due to accommodation of oxygen atoms in it. Obviously, the disordered stacking (quasi-$2H^{\delta}$) of structural units in this case results in the high diffusiveness of the superstructure reflections observed in the XRD powder patterns.

The Li^+ ion conductivity of solid solutions as prepared is lower, than that of $LiSi_2N_3$, which is evidently determined by the amount of Li^+ ions among the metal atoms.

Acknowledgements

The authors are grateful to Prof. A. Simon (Max-Planck-Institut für Festkörperforschung, Stuttgart) for the opportunity to perform high resolution electron microscopy investigations. The authors would like to thank Viola Duppel for practical electron microscopy work and the assistance in designing the figures.

References

1. W. SCHNICK, *Angew. Chem. Int. Ed. Engl.* **32** (1993) 806.
2. W. SCHNICK and H. HUPPERTZ, *Chem. Eur. J.* **3** (1997) 679.
3. H. P. BALDUS, O. WAGNER and M. JANSEN, *Mater. Res. Soc. Symp. Proc.* **271** (1992) 821; *Idem.*, patent EP0502399A2.
4. H. P. BALDUS, M. JANSEN and D. SPORN, *Science* **285** (1999) 699.
5. H. YAMANE, S. KIKKAWA and M. KOIZUMI, *Solid State Ionics* **25** (1987) 183.
6. C. C. LIANG, *J. Electrochem. Soc.* **120** (1973) 1289.
7. N. SATA, K. EBERMAN, K. EBERL and J. MAIER, *Nature* **408** (2000) 946.

8. S. ARAKAWA and S. HAYASHI, *J. Ceram. Soc. Japan* **108** (2000) 370.
9. J. T. S. IRVINE, A. J. FEIGHERY, D. P. FAGG and S. GARCÍA-MARTÍN, *Solid State Ionics* **136/137** (2000) 879.
10. D. P. THOMPSON, *Mater. Sci. Forum* **47** (1989) 21.
11. G. SCHNEIDER, L. J. GAUCKLER and G. PETZOW, *J. Amer. Ceram. Soc.* **63** (1980) 32.
12. K. H. JACK, in “Progress in Nitrogen Ceramics,” NATO Adv. Study Inst. Ser. E65 (Boston, 1983) p. 45.
13. H. HUPPERTZ and W. SCHNICK, *Z. Anorg. Allg. Chem.* **624** (1998) 371.
14. *Idem.*, *Angew. Chem.* **109** (1997) 2765.
15. K. A. ANDRIANOV, I. HAIDUC and L. M. KHANASHVILI, *Zh. Obshch. Khim.* **33** (1963) 2790.
16. H. ANDERSCH, Ph.D. thesis, University of Bonn, 1991.
17. P. A. STADELMAN, *Ultramicroscopy* **21** (1987) 131.
18. H. YAMANE, S. KIKKAWA and M. KOIZUMI, *Solid State Ionics* **15** (1985) 51.

Received 15 May 2001
and accepted 29 March 2002